Phase coexistence and connectivity in the apical membrane of polarized epithelial cells

Doris Meder*, Maria Joao Moreno†, Paul Verkade*, Winchil L. C. Vaz*†, and Kai Simons*‡

*Max Planck Institute of Molecular Cell Biology and Genetics, 01307 Dresden, Germany; and †Departamento de Química, Universidade de Coimbra, 3004-535 Coimbra, Portugal

Contributed by Kai Simons, November 14, 2005

Although it is well described in model membranes, little is known about phase separation in biological membranes. Here, we provide evidence for a coexistence of at least two different lipid bilayer phases in the apical plasma membrane of epithelial cells. Phase connectivity was assessed by measuring long-range diffusion of several membrane proteins by fluorescence recovery after photobleaching in two polarized epithelial cell lines and one fibroblast cell line. In contrast to the fibroblast plasma membrane, in which all of the proteins diffused with similar characteristics, in the apical membrane of epithelial cells the proteins could be divided into two groups according to their diffusion characteristics. At room temperature (≈25°C), one group showed fast diffusion and complete recovery. The other diffused three to four times slower and, more importantly, displayed only partial recovery. Only the first group comprises proteins that are believed to be associated with lipid rafts. The partial recovery is not caused by topological constraints (microvilli, etc.), cytoskeletal constraints, or protein–protein interactions, because all proteins show 100% recovery in fluorescence recovery after photobleaching experiments at 37°C. In addition, the raft-associated proteins cannot be coclustered by antibodies on the apical membrane at 12°C. The interpretation that best fits these data is that the apical membrane of epithelial cells is a phase-separated system with a continuous (percolating) raft phase <25°C in which isolated domains of the nonraft phase are dispersed, whereas at 37°C the nonraft phase becomes the continuous phase with isolated domains of the raft phase dispersed in it.

fluorescence recovery after photobleaching | rafts | paurdan | liquid-ordered | Madin–Darby-canine kidney

The domain organization of biological membranes is presently under intense scrutiny. In particular, the existence and role of sphingomyelin- and cholesterol-rich lipid bilayer phases, commonly known as rafts, have drawn much attention (1–5). Phase diagrams of model membrane systems made from ternary mixtures of sphingomyelin, 1-palmitoyl-2-oleoylphosphatidylcholine, and cholesterol show regions of fluid–fluid phase coexistence (6). The two fluid phases of special relevance are a liquid-ordered phase, characterized by high conformational and low translational order, and a liquid-disordered phase, characterized by low conformational and translational order (7, 8). The coexistence of these two phases has been visualized by several laboratories in giant unilamellar vesicles and supported lipid bilayers prepared from synthetic lipids. More importantly, giant unilamellar vesicles prepared from cell membrane lipid extracts (9) also show visible fluid–fluid phase coexistence. However, there was no direct evidence for phase separation in native cell membranes (2, 5). Glycosylphosphatidylinositol (GPI)-anchored proteins in the exoplasmic leaflet (10, 11) and lipid-anchored proteins in the cytoplasmic leaflet (12–14) of cell membranes were shown to be distributed nonrandomly in the plasma membrane with cluster sizes of 4–200 nm, but whether these correlate with lipid domains in a phase-separating system is not known. Indications for distinct lipid environments in living cells come from the measurements of different viscous drags for different bead-coupled proteins in the plasma membrane of fibroblasts (15) and from fluorescence anisotropy measurements of diphenyl chain-labeled phosphatidylcholine revealing liquid-ordered environments in the plasma membrane of mast cells (16) and *in vivo* images of liquid-ordered domains in macrophages labeled with 6-lauroyl-2-dimethylaminonaphthalene (17). However, the interpretations of the results obtained in all three cases may be questioned because of the invasive nature of the techniques. Also high-speed, single-molecule imaging has failed to detect lipid domains in resting fibroblasts (18).

In this work we have studied the long-range translational diffusion of several proteins associated with the apical membrane of epithelial cells [Madin-Darby-canine kidney (MDCK) and human colonic adenocarcinoma (Caco-2)]. Our data are consistent with the coexistence of lipid bilayer phases, a raft and a nonraft phase, in the apical membrane of epithelial cells.

Materials and Methods

DNA Constructs. Myristoylated and palmitoylated (MyrPalm)-yellow fluorescent protein (YFP), YFP-GL-GPI, linker of T cell activation (LAT)-WT-GFP, GFP-podocalyxin (PCX)-Δtail, vesicular stomatitis virus glycoprotein 3 (VSVG3)-GFP, and the placental alkaline phosphatase (PLAP) expression construct have been described (12, 19–23). LAT-TMD-GFP was derived from LAT-WT-GFP by PCR cloning of the ectodomain and transmembrane portion into the BamHI and SalI sites of the Clontech vector EGFP-N1, containing the lactase-phlorizin hydrolase signal sequence inserted into the NheI and PstI sites. YFP-low-density lipoprotein receptor (LDLR)-TMD was derived from LYFPGT46 (15) by PCR cloning of the YFP and the LDLR transmembrane domain and exchanging it for the original insert by using the KpnI and XbaI sites of LYFPGT46. Epidermal growth factor receptor (EGFR)-TMD-GFP was derived from the construct "vX" (24) by PCR cloning into the XhoI and KpnI sites of the Clontech vector pEGFP-N1. Wt-HA-M2-YFP contains full-length influenza virus hemagglutinin (HA) (strain A/WSN) fused to the cytoplasmic tail of influenza M2 protein cloned as a HindIII–NotI fragment into the Clontech vector pEYFP-N1.

Cell Culture and Transfection. PtK2 cells were grown in MEM with 10% FCS and nonessential amino acids. For experiments they were seeded sparsely onto glass coverslips 2 days in advance and transfected with Fugene reagent, according to the manufacturer's suggestions, the next day. MDCK II cells were grown in MEM with 5% FCS. For terminal polarization, cells were seeded onto Transwell filters (Corning Costar) in MEM with 10% FCS

Conflict of interest statement: No conflicts declared.

Freely available online through the PNAS open access option.

Abbreviations: EGFR, epidermal growth factor receptor; FRAP, fluorescence recovery after photobleaching; GPI, glycosylphosphatidylinositol; LAT, linker of T cell activation; LDLR, low-density lipoprotein receptor; MDCK, Madin-Darby-canine kidney; MyrPalm, myristoylated and palmitoylated; PCX, podocalyxin; PLAP, placental alkaline phosphatase; VSVG, vesicular stomatitis virus glycoprotein; YFP, yellow fluorescent protein.

‡To whom correspondence should be addressed. E-mail: simons@mpi-cbg.de.

and cultured for 3 days. MDCK cells were transfected by electroporation [5 μg DNA for 10^6 cells, Amaxa (Gaithersburg, MD) technology] before seeding onto filters, or, for expression of VSVG3-GFP, infected with replication-deficient adenovirus (Qbiogene, Heidelberg) 1 day before the experiment. MDCK II cells stably expressing PLAP were a gift from D. Brown (Stony Brook University, New York) (23). Caco-2 cells were grown in DMEM with 10% FCS. Cells were allowed to polarize on Transwell filters (Corning Costar) for 6 days, and were infected with replication-deficient adenovirus 1 day before the experiment. BHK cells were grown in G-MEM with 10% tryptose phosphate and 5% FCS. For experiments they were seeded sparsely onto glass coverslips 2 days in advance and infected with replication-deficient adenovirus 1 day before the experiment.

Fluorescence Recovery After Photobleaching (FRAP) Measurements and Analysis. A circular spot, covering up to 0.5% of the surface in PtK2 cells and up to 5% of the apical membrane surface in MDCK and Caco-2 cells, was bleached with high laser power, and the subsequent recovery of fluorescence was recorded with 1/100–1/50 of the bleaching laser power for 3–4 min. FRAP recordings were carried out in CO_2-independent medium (Gibco) with 10% FCS on a Zeiss LSM 510 microscope at room temperature or 37°C. The experimental data were corrected for bleaching occurring during recording, normalized to a prebleach fluorescence intensity $I_i = 1$, and fitted to a 2D diffusion model (25, 26). The theoretical fit adjusted the characteristic recovery time, the postbleach fluorescence intensity immediately after photobleaching, I_0, and the fluorescence intensity at infinite time after photobleaching, I_∞. The apparent diffusion coefficient, D (calculated from the characteristic recovery time), and the fraction recovered [given by $(I_\infty - I_0)/(I_i - I_0)$] were derived from the theoretical fits for every experiment and subsequently averaged. The curves displayed in Fig. 2 were calculated from the averaged experimentally determined parameters (D and the fraction recovered) for a fixed bleaching spot radius of 1 μm and an initial postbleach fluorescence intensity $I_0 = 0$.

Antibody Clustering and Immunoelectron Microscopy. Antibody clustering and immunoelectron microscopy were performed as described (27). The distance of HA toward a PLAP cluster (see Fig. 3*G*) was measured across a straight line from a HA-labeled gold particle or cluster toward the nearest PLAP cluster.

Results

To assess phase connectivity, we have measured the long-range diffusion of proteins associated with the plasma membrane by using confocal FRAP as a noninvasive method (28). Although a "phase" can be defined only in a system at equilibrium and, under certain conditions, in the steady state, we shall apply the term here to the nonequilibrium system of a cell membrane and use it to define coexisting domains or lipid environments of distinct physical and chemical properties. Because earlier similar studies using FRAP were not able to resolve phase separation in fibroblast plasma membranes (29), we chose to study the diffusion characteristics in the apical membrane of epithelial cells, namely MDCK or Caco-2 cells, which have a different lipid composition (30) and possibly also a different domain organization from that of fibroblast plasma membranes. To this end, fluorescent proteins of different topologies (Fig. 1 and Fig. 6, which is published as supporting information on the PNAS web site) were expressed on the cell surface, a small fraction (≤5%) was bleached, and the subsequent fluorescence recovery resulting from exchange between bleached and nonbleached molecules was recorded, normalized, and fitted to a 2D diffusion model (25, 26). From a variety of possible probes we stringently selected those that at steady state showed mainly apical membrane localization on polarized MDCK cells with no staining of the endoplasmic reticulum or other organelles close to the plasma membrane.

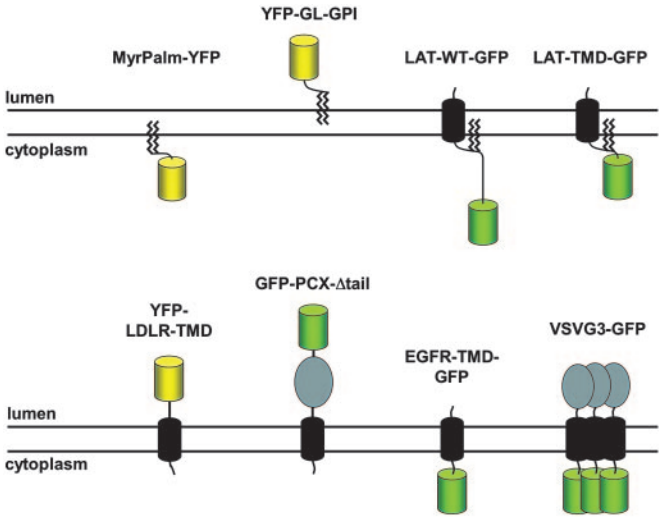

Fig. 1. Overview of the fluorescent membrane proteins used for FRAP measurements. There are two lipid-anchored probes: MyrPalm-YFP is a MyrPalm monomeric YFP anchored in the cytoplasmic leaflet of the plasma membrane, and YFP-GL-GPI is a GPI-anchored, glycosylated YFP anchored in the exoplasmic leaflet. All other probes are transmembrane proteins. These include: (*i*) proteins with small ectodomains and cytoplasmic GFP, like full-length LAT (LAT-WT-GFP), a version of the same protein in which the cytoplasmic tail has been deleted (LAT-TMD-GFP), and the transmembrane domain of EGFR with the juxtamembrane part of the ectodomain (EGFR-TMD-GFP); (*ii*) proteins with GFP or YFP fused to ectodomains of variable size, like the transmembrane domain of LDLR, N-terminally fused to glycosylated YFP (YFP-LDLR-TMD) and a N-terminally GFP-tagged PCX variant in which the cytoplasmic tail has been deleted (GFP-PCX-Δtail), and (*iii*) VSVG C-terminally fused to GFP, which trimerizes and is targeted apically (VSVG3-GFP). Yellow or green cylinders indicate YFP and GFP moieties, respectively.

All Probes Diffuse with Similar Characteristics in the Plasma Membrane of PtK2 Cells, But Not in the Apical Membrane of Epithelial Cells. FRAP experiments were routinely performed at room temperature (≈25°C) to minimize membrane deformations caused by temperature gradients and the influence of membrane traffic events on fluorescence recovery (31). The apparent diffusion coefficient D and the percentage recovery were derived from the fluorescence intensity at "infinite" time after photobleaching, I_∞, calculated by the theoretical fit (25, 26) and not from a visual examination of the experimental curves that were rarely followed until recovery was complete.

In the plasma membrane of fibroblasts (PtK2 cells), all fluorescent proteins tested in FRAP experiments had similar D values and recovered to 100% (Fig. 2*A*), similar to previous results obtained on different fibroblast plasma membranes (29). When analogous experiments were performed on the apical membrane of terminally polarized MDCK cells, the situation was completely different. Based on the characteristics of the FRAP curves, the proteins could be categorized into two groups: one that diffused fast and recovered to nearly 100%, and one that diffused three to four times more slowly and recovered only partially. All proteins belonging to this first group, YFP-GL-GPI, LAT-WT-GFP, and LAT-TMD-GFP (Fig. 2*B*, red), have by presently used criteria been associated with rafts (19, 32, 33), whereas the proteins belonging to the second group, GFP-PCX-Δtail, EGFR-TMD-GFP, and VSVG3-GFP (Fig. 2*B*, blue) have not (15, 19, 21). YFP-LDLR-TMD displayed a mixed behavior, diffusing fast but recovering only to 80%. Furthermore, proteins of the first

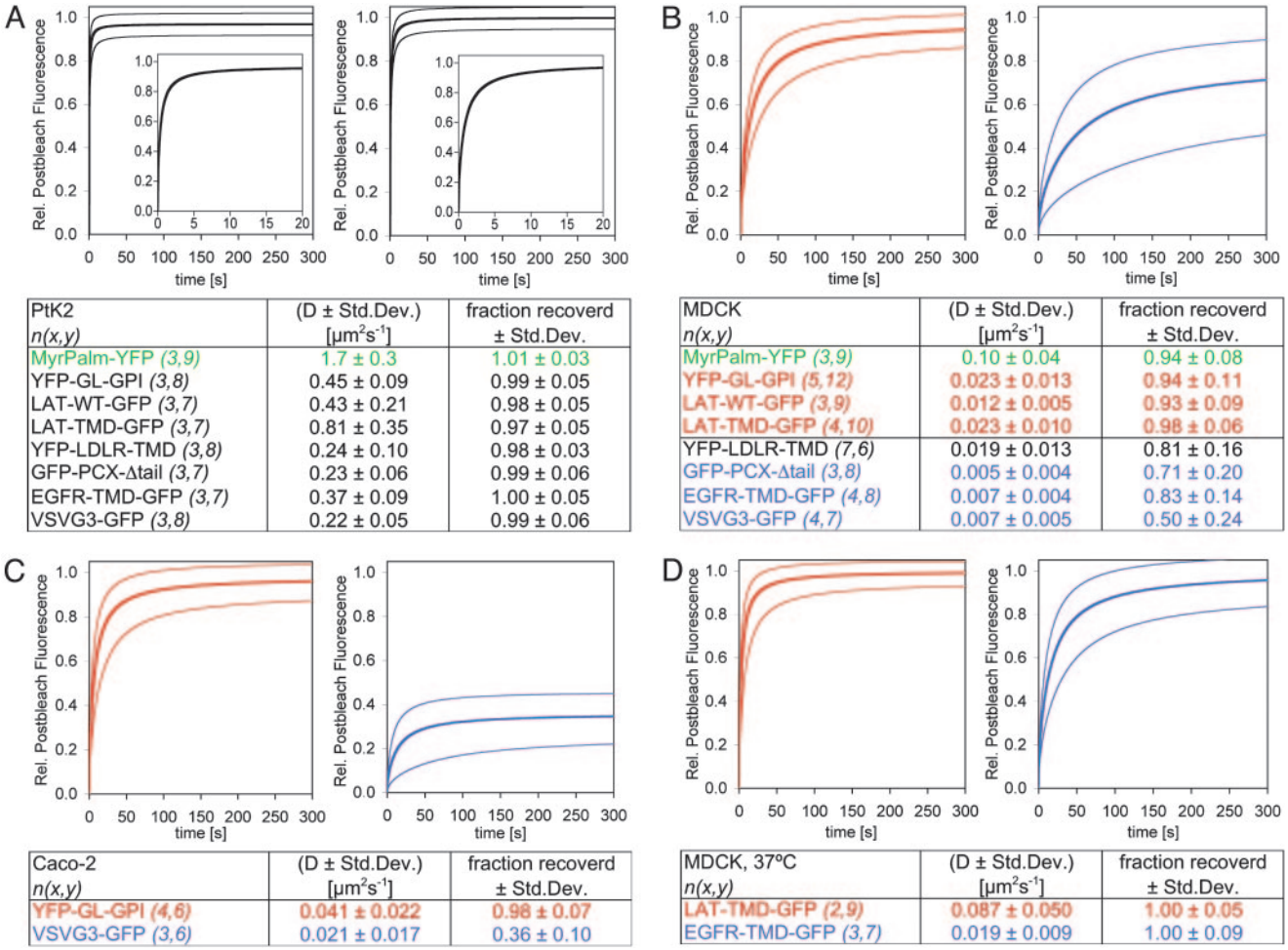

PtK2 *n(x,y)*	(D ± Std.Dev.) [$\mu m^2 s^{-1}$]	fraction recoverd ± Std.Dev.
MyrPalm-YFP *(3,9)*	1.7 ± 0.3	1.01 ± 0.03
YFP-GL-GPI *(3,8)*	0.45 ± 0.09	0.99 ± 0.05
LAT-WT-GFP *(3,7)*	0.43 ± 0.21	0.98 ± 0.05
LAT-TMD-GFP *(3,7)*	0.81 ± 0.35	0.97 ± 0.05
YFP-LDLR-TMD *(3,8)*	0.24 ± 0.10	0.98 ± 0.03
GFP-PCX-Δtail *(3,7)*	0.23 ± 0.06	0.99 ± 0.06
EGFR-TMD-GFP *(3,7)*	0.37 ± 0.09	1.00 ± 0.05
VSVG3-GFP *(3,8)*	0.22 ± 0.05	0.99 ± 0.06

MDCK *n(x,y)*	(D ± Std.Dev.) [$\mu m^2 s^{-1}$]	fraction recoverd ± Std.Dev.
MyrPalm-YFP *(3,9)*	0.10 ± 0.04	0.94 ± 0.08
YFP-GL-GPI *(5,12)*	0.023 ± 0.013	0.94 ± 0.11
LAT-WT-GFP *(3,9)*	0.012 ± 0.005	0.93 ± 0.09
LAT-TMD-GFP *(4,10)*	0.023 ± 0.010	0.98 ± 0.06
YFP-LDLR-TMD *(7,6)*	0.019 ± 0.013	0.81 ± 0.16
GFP-PCX-Δtail *(3,8)*	0.005 ± 0.004	0.71 ± 0.20
EGFR-TMD-GFP *(4,8)*	0.007 ± 0.004	0.83 ± 0.14
VSVG3-GFP *(4,7)*	0.007 ± 0.005	0.50 ± 0.24

Caco-2 *n(x,y)*	(D ± Std.Dev.) [$\mu m^2 s^{-1}$]	fraction recoverd ± Std.Dev.
YFP-GL-GPI *(4,6)*	0.041 ± 0.022	0.98 ± 0.07
VSVG3-GFP *(3,6)*	0.021 ± 0.017	0.36 ± 0.10

MDCK, 37°C *n(x,y)*	(D ± Std.Dev.) [$\mu m^2 s^{-1}$]	fraction recoverd ± Std.Dev.
LAT-TMD-GFP *(2,9)*	0.087 ± 0.050	1.00 ± 0.05
EGFR-TMD-GFP *(3,7)*	0.019 ± 0.009	1.00 ± 0.09

Fig. 2. In FRAP experiments, all probes recover with similar kinetics on the plasma membrane of PtK2 cells, but not on the apical membrane of MDCK and Caco-2 cells. (*A*) PtK2 cells grown on coverslips. (*B* and *D*) MDCK cells polarized on filter supports for 3 days. (*C*) Caco-2 cells polarized on filter supports for 6 days. A circular spot of 10–40 μm^2 in a flat region of the cell (*A*) or a 4- to 10-μm^2 spot in the center of the apical membrane (*B–D*) was bleached, and fluorescence intensities were recorded. The experiment was performed at room temperature (*A–C*) or 37°C (*D*). The raw experimental data were corrected for bleaching during the recording, normalized, and fitted to a 2D diffusion model (25, 26). The calculated FRAP curve, based on experimentally determined average values of *D* and percentage recovery (heavy line), and the average ± 1 SD (upper and lower fine lines, respectively) is plotted for LAT-TMD-GFP (*Left*) and EGFR-TMD-GFP (*Right*) (*A*, *B*, and *D*) and YFP-GL-GPI (*Left*) and VSVG3-GFP (*Right*) (*C*). Shown are the calculated apparent diffusion coefficient, *D*, and the fraction that recovered as averages with SDs for all theoretical fits. Both are derived from the theoretical fit, not by visual examination of the experimental curve. The number of FRAP curves *n* used for the theoretical analysis is given by x = number of independent experiments and y = average number of cells recorded per experiment ($n = x \times y$). Green indicates surface scooting diffusion; red indicates so-called raft proteins, and blue indicates so-called nonraft proteins.

group diffused with nearly identical kinetics (low SDs), whereas proteins of the second group displayed very different diffusion characteristics, which varied between cells and resulted in high SDs (Fig. 2 *B* and *C*). The appearance of two distinct groups of proteins with different long-range diffusion characteristics is not unique to MDCK cells, but was observed on the apical membrane of Caco-2 cells as well (Fig. 2*C*), and may be a general feature of the apical membrane of epithelial cells.

In all cell types examined, the MyrPalm-YFP diffused an order of magnitude faster than the fastest diffusing membrane-associated proteins (Fig. 2 *A* and *B*). This behavior is expected for "surface hopping," in which the protein does not diffuse exclusively in the membrane-anchored form within the plane of the bilayer. The two lipid anchors probably behave like independent single chains with rapid insertion/desorption kinetics (34) that favor fast exchange between the membrane-anchored and surface "scooting" modes of diffusion. The recovery kinetics for this protein are thus independent of membrane domain organization and reflect the surface area. Consequently, in the apical membrane of MDCK cells, where the surface is greatly enlarged by microvilli, *D* of MyrPalm-YFP was ≈10 times lower than in PtK2 cells. This result is in agreement with morphometric analyses showing that the apical membrane surface area is enlarged 8-fold by microvilli (35).

Obstructed Diffusion Is Not Caused by Biological Constraints. The obstructed diffusion of the second group of proteins indicates that they do not have full access to the whole plasma membrane but could, in fact, reside in domains that are isolated from the remaining membrane plane. Cell surface topology should be considered as one explanation for the observed diffusion patterns. A preferential localization to microvilli should result in slow diffusion. Immunoelectron microscopy, however, demonstrated an even distribution of all proteins over planar and microvillar membrane surfaces (Fig. 7, which is published as supporting information on the PNAS web site). The different diffusion behaviors thus do not originate from topological constraints.

Obstructed Diffusion Is Temperature-Dependent. There could be two other explanations for the obstructed diffusion. (*i*) The proteins could engage into specific protein–protein interactions in the apical membrane of epithelial cells, which link them to the cytoskeleton and thereby hinder their diffusion. (*ii*) The plasma membrane of epithelial cells displays phase separation into different lipid environments and the proteins reside in a phase that is not continuous (i.e., nonpercolating), but exists as isolated domains. To distinguish between the two, we performed FRAP experiments at 37°C. Protein–protein association constants are expected to change monotonically with temperature. Thus, if the partial recovery observed for some proteins was caused by protein–protein association (including direct or indirect association with the cytoskeleton), both D and the fractional recovery would increase, but a transition from partial recovery to full recovery might not be reasonably expected. On the other hand, if in a two-phase system the percolation threshold was crossed between 25°C and 37°C, i.e., the continuous phase at 25°C would become the discontinuous phase at 37°C, those proteins that showed partial recovery at 25°C would show full recovery at 37°C.

Strikingly, this switch from partial to full recovery is exactly what we observed. Results for LAT-TMD-GFP (a raft-associated protein) and EGFR-TMD-GFP (a nonraft protein) diffusion in MDCK cells are presented in Fig. 2*D*. Both are seen to diffuse faster at 37°C than at 25°C, but EGFR-TMD-GFP, which recovered only partially at 25°C, recovers completely at 37°C, which indicates that at the higher temperature this protein encounters itself in a continuous phase and that LAT-TMD-GFP now is in a discontinuous phase. However, it also shows complete recovery in the FRAP experiment at 37°C, which is easily explained if the partition coefficient (K_P) for this so-called raft protein between a raft and a nonraft phase is assumed to have a value close to 1, granting it equal access to both phases.

A closer examination of the values of D for both proteins is also informative. For LAT-TMD-GFP, D increased 3.8-fold and for EGFR-TMD-GFP it increased 2.7-fold from 25°C to 37°C. The two proteins are topologically very similar (Fig. 1), and their diffusion coefficients should be indistinguishable in a homogeneous membrane. Within the context of our interpretation, the 3-fold lower value of D for EGFR-TMD-GFP compared with LAT-TMD-GFP at 25°C (and not just the incomplete fluorescence recovery) is caused by constraints resulting from the nonpercolating nature of the phase for which EGFR-TMD-GFP shows a partitioning preference. When this phase became a percolating phase (at 37°C), the diffusion coefficient would be expected to increase by about an order of magnitude, which is not the case. The lower increase for EGFR-TMD-GFP may be attributed to obstacles in its path at 37°C consisting of disconnected raft domains that are now dispersed in the continuous nonraft phase.

The Special Domain Organization of the Apical Membrane Is Also Revealed by Antibody Crosslinking. Another method that has been used to indirectly visualize phase separation of cell membranes is antibody crosslinking at 12°C. As previously published, the simultaneous addition of antibodies against two components of lipid rafts (1), here influenza virus HA and PLAP, led to their coclustering into visible domains that were segregated from the bulk of the membrane on the cell surface of a fibroblast (27) (Fig. 3 *C* and *G*). If the same experiment was performed on the apical membrane of MDCK cells, the outcome was entirely different. The clusters were less well defined and there was almost no coclustering of the two raft components (Fig. 3 *D* and *G*). Immunoelectron microscopy confirmed this finding and revealed that clusters on the apical membrane of MDCK cells were much smaller than those on the surface of BHK cells (36) (Fig. 3 *E*–*G*).

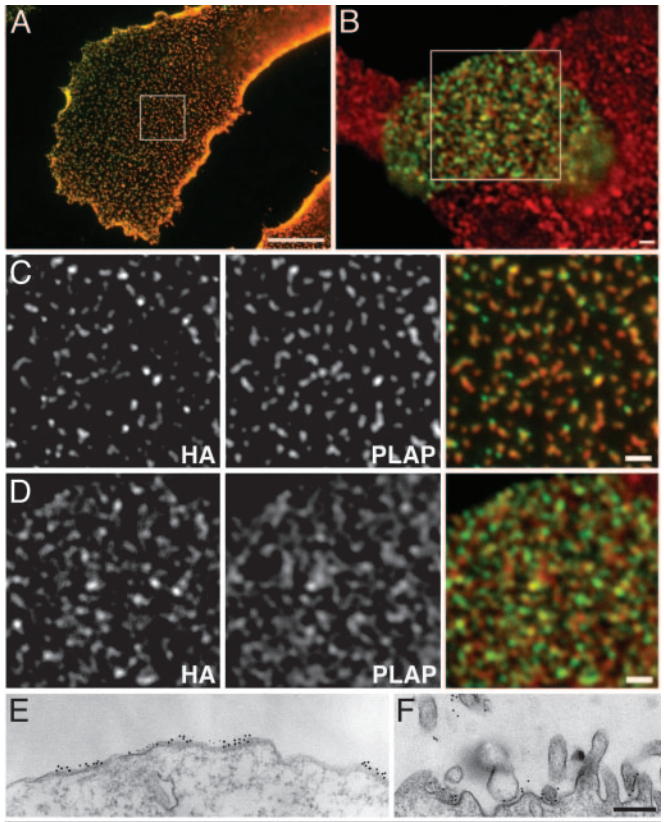

G	BHK	MDCK
PLAP cluster size	405.0 ± 39.8 nm	61.5 ± 2.6 nm
Distance of HA towards a PLAP cluster	35.8 ± 3.0 nm	84.6 ± 10.7 nm

Fig. 3. The special domain organization of the apical membrane is also revealed by antibody crosslinking. BHK cells grown on coverslips and expressing PLAP with the HA construct wtHA-M2-YFP (*A* and *C*) or alone (*E*) are shown. MDCK cells stably expressing PLAP polarized on filter supports for 5 days (*F*) and infected with adenovirus expressing wtHA-M2-YFP (*B* and *D*) are shown. Crosslinking was performed on living cells at 12°C by simultaneous addition of antibodies. Whereas the two raft proteins coclustered on the plasma membrane of BHK cells (*C*), they segregated on the apical membrane of MDKC cells (*D*). Crosslinking of PLAP led to the formation of large clusters on the plasma membrane of BHK cells (*E* and *G*) compared with small clusters on the apical membrane of MDCK cells (*F* and *G*). Results in *G* were derived from electron microscopy experiments. (Scale bars: *A* and *B*, 10 μm; *C* and *D*, 1 μm; and *E* and *F*, 250 nm.)

Discussion

The question we set out to answer was: "Is there fluid–fluid phase coexistence in native cell membranes?"

In a liquid with fluid–fluid phase coexistence the solutes (in our case the membrane proteins) will be heterogeneously distributed depending on their preferences for one or the other of the coexisting fluid phases as a solvent. This solvent preference will be influenced by protein–protein association, but because very little is known about this phenomenon, we shall ignore it for the present discussion. In the limit of low concentration, protein heterogeneity will be determined by the partition coefficient (K_P), the ratio of the concentrations of a given protein in the two coexisting phases at equilibrium. In the limit of high protein concentration, the molar solubility of the proteins in each of the phases also becomes important. From a dynamic perspective, K_P is the probability with which a protein molecule at a boundary between two phases will cross that boundary although it says nothing about the rate at which it does so.

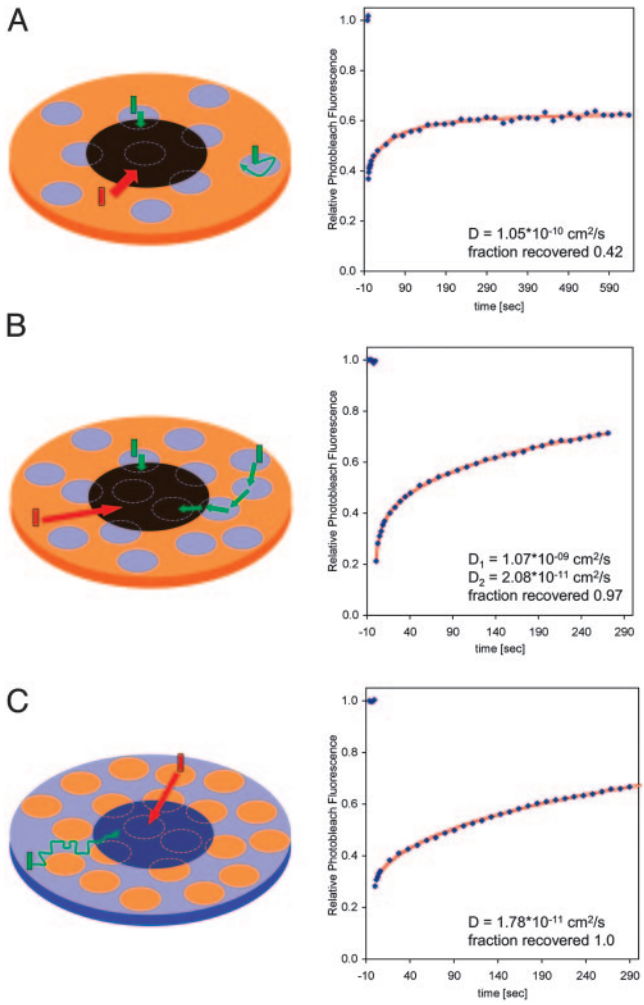

Fig. 4. Three recovery kinetics characteristic for a system close to the percolation threshold. Examples from nonraft proteins in the apical membrane of MDCK cells, GFP-PCXΔtail (*A* and *C*) and EGFR-TMD-GFP (*B*) are shown. Each curve shows a single experiment (blue diamonds) with its theoretical fit (red line). Raft proteins are red bars. The raft phase is displayed in orange, the nonraft phase is displayed in blue, and nonraft proteins are green bars. The models are very simplified with respect to domain size and shape for purposes of elucidating the process and should not be understood literally.

Fluid–fluid phase coexistence imparts a new physical property to the membrane: the percolation threshold. One of the fluid phases is continuous (percolating) and the other is discontinuous and can exist as small domains dispersed in the continuous fluid (37–39). Two fluid phases in a membrane may mutually interconvert because they are made up of (different proportions of) the same chemical constituents. In this case, changes in the chemical composition, lateral pressure, and/or temperature of the membrane will cause interconversion between the two fluids, i.e., the mass fraction of one of them will grow at the expense of the other. This process may lead to a reduction in the mass fraction of the continuous phase and growth in the mass fraction of the discontinuous phase to the point where the previously discontinuous phase becomes continuous and the previously continuous phase is discontinuous. The point (in terms of chemical composition, lateral pressure, temperature, etc.) at which this happens is the percolation threshold.

Let us consider how the above can be expected to affect long-range diffusion of the proteins in a membrane with phase coexistence. When a protein diffusing in a given phase reaches

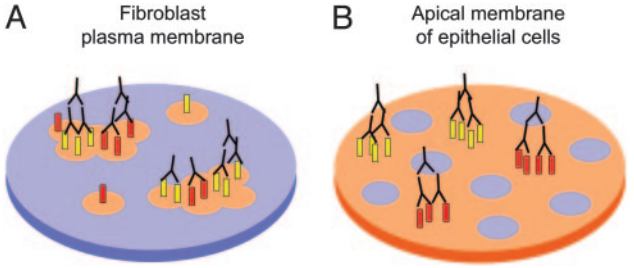

Fig. 5. A model for the domain organization of the apical membrane of epithelial cells compared with the plasma membrane of a fibroblast (see discussion in the text). The raft phase is displayed in orange, the nonraft phase is displayed in blue, and raft proteins are yellow and red bars.

a boundary between that phase and a domain of the coexisting phase, that boundary will constitute an obstacle to its free diffusion depending on K_P. In the limit of $K_P = 0$, i.e., the protein does not partition into the phase on the other side of the boundary, the phase boundary is an insurmountable barrier and the protein will have to find a free path around the obstacle, thereby lowering the apparent long-range diffusion coefficient (D) measured in a FRAP experiment. If the impenetrable domain is small, the reduction will be less. If no free path can be found, the protein is trapped in a nonpercolating domain, which manifests itself in fractional recovery. For $K_P = 1$ the boundary is penetrable and the value of D obtained in a FRAP experiment is a weighted mean of D in the two coexisting phases. For $K_P \ll 1$ the boundary is not completely impenetrable and a combination of the consequences of having to walk around the boundary and its penetration may be expected. In a FRAP experiment $K_P \ll 1$ leads to anomalous subdiffusion (40, 41).

FRAP experiments on the diffusion of raft and nonraft proteins in the plasma membranes of fibroblasts indicated that raft partitioning of proteins was not a static phenomenon but they were unable to distinguish between the nonexistence of rafts and the dynamic partitioning of proteins between a raft and a nonraft phase (29). Our present results on PtK2 cell membranes confirm this observation and conclusion (Fig. 2*A*). If rafts do exist in these membranes, they must be small (small effect on D of nonraft proteins) and the raft proteins must have $K_P \approx 1$ (no significant reduction in D and full recovery). In the apical membrane of epithelial cells at 25°C, however, the situation is very different (Fig. 2 *B* and *C*). Raft proteins display complete fluorescence recovery and not significantly altered values of D (when surface roughness is taken into account), which confirms the assumption that $K_P \approx 1$ for partitioning of these proteins between raft and nonraft phases. Nonraft proteins show incomplete fluorescence recoveries in the FRAP experiments and significantly reduced values of D even after taking surface roughness into account (Fig. 2 *B* and *C*). In fact, FRAP curves of these proteins exhibit three types of behavior (Fig. 4) that are characteristic of phase coexistence and the poor partitioning of these proteins into a raft phase ($K_P \ll 1$). Few isolated domains of a nonraft phase in a percolating raft phase give rise to an unusually high D and incomplete recovery that results only from those domains straddling the perimeter of the bleached spot (Fig. 4*A*). A large number of isolated nonraft domains in a continuous raft phase gives rise to a combination of rapid recovery (high D) from domains that straddle the perimeter of the FRAP spot, and slow recovery (low D) resulting from infrequent "island hopping" at a rate permitted by the low value of K_P (Fig. 4*B*). In a continuous nonraft phase with a large number of raft domains, the low value of K_P results in a raft-obstacle-retarded recovery and a very low value of the apparent D (Fig. 4*C*). The exact physical description of the

system is, of course, much more complicated so that Fig. 4 and the above description of it are only qualitative.

Finally, at 37°C all proteins show complete recovery in the FRAP experiments on the apical MDCK cell membrane. This result could be understood as follows. The system has crossed a percolation threshold between 25°C and 37°C so that the continuous raft phase at 25°C is discontinuous at 37°C. For raft protein diffusion D or fractional recovery is not affected because $K_P \approx 1$. For nonraft proteins, their preferred phase is now continuous (full recovery), but they face obstacles in the form of raft domains that they penetrate only poorly, resulting in a smaller increase in D than might be expected for the increased temperature (see *Results*).

Antibody crosslinking experiments on fibroblast and apical MDCK membranes are in agreement with our interpretations of the FRAP data. These experiments, performed at 12°C to prevent internalization of membrane clusters, should show a domain organization that corresponds to the phase diagram of the respective membrane at 12°C. In fibroblasts, crosslinking of a raft antigen leads to coalescence of isolated raft domains into large clusters with several different raft proteins (27) (Fig. 5*A*). In apical MDCK membranes, the raft phase is a percolating phase so that antibody crosslinking leads to small clusters made up only from the specific antigen without coclustering of other raft proteins (Fig. 5*B*).

Conclusions

Phase separation and the formation of lipid domains in cell membranes have remained elusive largely because of the lack of reliable noninvasive methods to study their existence and the size, composition, and dynamics of lipid domains. FRAP, as we have used it, has the advantage of simultaneously examining a large population of protein molecules in a noninvasive way. It has been successfully used in the past to examine the domain organization of model membranes with phase coexistence (28, 38, 39, 42). Our study shows domain coexistence *in vivo* in cell membranes.

We thank N. Hirokawa (University of Tokyo, School of Medicine, Tokyo), P. Keller (Meso Scale Discovery, Dresden, Germany), L. Samelson (National Institutes of Health, Bethesda), R. Tsien (University of California at San Diego), and M. Yamabhai (Suranaree University of Technology, Nakhorn Ratchasima, Thailand) for cDNA constructs; D. Brown for PLAP-MDCK cells; and J. Howard, F. Jülicher, L. Pelkmans, and P. Schwille for critical reading of the manuscript. This work was supported by European Union Grant HPRN-CT-2002-00259, Transregio Grant SFB-TR13-TPA1, and research grants from the Portuguese Ministry of Sciences and Higher Education through Programa Operacional Ciência, Tecnologia, Inovação. W.L.C.V. acknowledges support from the Portuguese Ministry of Sciences and Higher Education for his sabbatical leave at the Max Planck Institute of Molecular Cell Biology and Genetics.

1. Simons, K. & Ikonen, E. (1997) *Nature* **387,** 569–572.
2. Edidin, M. (2003) *Annu. Rev. Biophys. Biomol. Struct.* **32,** 257–283.
3. Silvius, J. R. (2003) *Biophys. J.* **85,** 1034–1045.
4. Simons, K. & Vaz, W. L. (2004) *Annu. Rev. Biophys. Biomol. Struct.* **33,** 269–295.
5. Munro, S. (2003) *Cell* **115,** 377–388.
6. de Almeida, R. F., Fedorov, A. & Prieto, M. (2003) *Biophys. J.* **85,** 2406–2416.
7. Ipsen, J. H., Karlstrom, G., Mouritsen, O. G., Wennerstrom, H. & Zuckermann, M. J. (1987) *Biochim. Biophys. Acta* **905,** 162–172.
8. Ipsen, J. H., Mouritsen, O. G. & Zuckermann, M. J. (1989) *Biophys. J.* **56,** 661–667.
9. Dietrich, C., Bagatolli, L. A., Volovyk, Z. N., Thompson, N. L., Levi, M., Jacobson, K. & Gratton, E. (2001) *Biophys. J.* **80,** 1417–1428.
10. Friedrichson, T. & Kurzchalia, T. V. (1998) *Nature* **394,** 802–805.
11. Sharma, P., Varma, R., Sarasij, R. C., Ira, Gousset, K., Krishnamoorthy, G., Rao, M. & Mayor, S. (2004) *Cell* **116,** 577–589.
12. Zacharias, D. A., Violin, J. D., Newton, A. C. & Tsien, R. Y. (2002) *Science* **296,** 913–916.
13. Prior, I. A., Muncke, C., Parton, R. G. & Hancock, J. F. (2003) *J. Cell Biol.* **160,** 165–170.
14. Lommerse, P. H., Blab, G. A., Cognet, L., Harms, G. S., Snaar-Jagalska, B. E., Spaink, H. P. & Schmidt, T. (2004) *Biophys. J.* **86,** 609–616.
15. Pralle, A., Keller, P., Florin, E. L., Simons, K. & Horber, J. K. (2000) *J. Cell Biol.* **148,** 997–1008.
16. Gidwani, A., Holowka, D. & Baird, B. (2001) *Biochemistry* **40,** 12422–12429.
17. Gaus, K., Gratton, E., Kable, E. P., Jones, A. S., Gelissen, I., Kritharides, L. & Jessup, W. (2003) *Proc. Natl. Acad. Sci. USA* **100,** 15554–15559.
18. Kusumi, A., Koyama-Honda, I. & Suzuki, K. (2004) *Traffic* **5,** 213–230.
19. Keller, P., Toomre, D., Diaz, E., White, J. & Simons, K. (2001) *Nat. Cell Biol.* **3,** 140–149.
20. Bunnell, S. C., Hong, D. I., Kardon, J. R., Yamazaki, T., McGlade, C. J., Barr, V. A. & Samelson, L. E. (2002) *J. Cell Biol.* **158,** 1263–1275.
21. Meder, D., Shevchenko, A., Simons, K. & Fullekrug, J. (2005) *J. Cell Biol.* **168,** 303–313.
22. Nakata, T., Terada, S. & Hirokawa, N. (1998) *J. Cell Biol.* **140,** 659–674.
23. Brown, D. A., Crise, B. & Rose, J. K. (1989) *Science* **245,** 1499–1501.
24. Yamabhai, M. & Anderson, R. G. (2002) *J. Biol. Chem.* **277,** 24843–24846.
25. Axelrod, D., Koppel, D. E., Schlessinger, J., Elson, E. & Webb, W. W. (1976) *Biophys. J.* **16,** 1055–1069.
26. Soumpasis, D. M. (1983) *Biophys. J.* **41,** 95–97.
27. Harder, T., Scheiffele, P., Verkade, P. & Simons, K. (1998) *J. Cell Biol.* **141,** 929–942.
28. Vaz, W. L., Melo, E. C. & Thompson, T. E. (1989) *Biophys. J.* **56,** 869–876.
29. Kenworthy, A. K., Nichols, B. J., Remmert, C. L., Hendrix, G. M., Kumar, M., Zimmerberg, J. & Lippincott-Schwartz, J. (2004) *J. Cell Biol.* **165,** 735–746.
30. Simons, K. & van Meer, G. (1988) *Biochemistry* **27,** 6197–6202.
31. Bacia, K., Scherfeld, D., Kahya, N. & Schwille, P. (2004) *Biophys. J.* **87,** 1034–1043.
32. Shogomori, H., Hammond, A. T., Ostermeyer-Fay, A. G., Barr, D. J., Feigenson, G. W., London, E. & Brown, D. A. (2005) *J. Biol. Chem.* **280,** 18931–18942.
33. Janes, P. W., Ley, S. C. & Magee, A. I. (1999) *J. Cell Biol.* **147,** 447–461.
34. Sampaio, J. L., Moreno, M. J. & Vaz, W. L. (2005) *Biophys. J.* **88,** 4064–4071.
35. Butor, C. & Davoust, J. (1992) *Exp. Cell Res.* **203,** 115–127.
36. Verkade, P., Harder, T., Lafont, F. & Simons, K. (2000) *J. Cell Biol.* **148,** 727–739.
37. Vaz, W. L. & Almeida, P. F. (1993) *Curr. Opin. Struct. Biol.* **3,** 482–488.
38. Almeida, P. F., Vaz, W. L. & Thompson, T. E. (1992) *Biochemistry* **31,** 7198–7210.
39. Vaz, W. L. (1994) *Biophys. Chem.* **50,** 139–145.
40. Feder, T. J., Brust-Mascher, I., Slattery, J. P., Baird, B. & Webb, W. W. (1996) *Biophys. J.* **70,** 2767–2773.
41. Saxton, M. J. (2001) *Biophys. J.* **81,** 2226–2240.
42. Ratto, T. V. & Longo, M. L. (2002) *Biophys. J.* **83,** 3380–3392.